Bimetallic MNi/Al2O3–La catalysts (M = Pt, Cu) for acetone steam reforming: Role of M on catalyst structure and activity

ARTICLE *in* APPLIED CATALYSIS A GENERAL · MARCH 2014

Impact Factor: 3.94 · DOI: 10.1016/j.apcata.2013.09.056

Applied Catalysis A: General 474 (2014) 168–177

Contents lists available at ScienceDirect

Applied Catalysis A: General

journal homepage: www.elsevier.com/locate/apcata

Bimetallic MNi/Al_2O_3-La catalysts (M = Pt, Cu) for acetone steam reforming: Role of M on catalyst structure and activity

R.M. Navarro[a,*], R. Guil-Lopez[a], J.M. Gonzalez-Carballo[a], A. Cubero[a], A.A. Ismail[b,c], S.A. Al-Sayari[b], J.L.G. Fierro[a,*]

[a] Grupo de Energía y Química Sostenibles, ICP-CSIC, C/ Marie Curie 2, Cantoblanco, 28049 Madrid, Spain
[b] Advanced Materials and Nano Research Centre, Najran University, Najran 11001, Saudi Arabia
[c] Advanced Materials Department, Central Metallurgical R&D Institute, CMRDI, Helwan 11421, Egypt

ARTICLE INFO

Article history:
Received 1 April 2013
Received in revised form 6 September 2013
Accepted 11 September 2013
Available online 1 November 2013

Keywords:
Nickel catalysts
Platinum
Copper
Alumina
Lanthanum
Hydrogen production
Bio-oil
Acetone
Steam reforming

ABSTRACT

The effect of Pt and Cu addition on the behaviour of Ni catalysts supported on Al_2O_3 modified with La for acetone steam reforming (as model molecule of bio-oil) was studied. Catalytic activity was found to depend strongly on the bimetallic formulation, achieving the bimetallic PtNi catalyst almost complete gasification of the acetone. The characterization results achieved with XRD, TPR and XPS showed differences in surface metal concentrations which depend on the presence of Pt or Cu in catalysts composition. The decrease in activity observed for the bimetallic CuNi catalyst is associated with changes in the acetone reaction mechanism due to the presence of metallic copper since formation of CuNi alloy was not formed in this catalyst. In the case of bimetallic PtNi catalyst, a lower carbon deposition and a higher thermal stability of the Ni crystallites under reaction conditions was observed with respect to monometallic Ni reference catalyst. It is suggested that the better dispersion of metallic nickel crystallites together with the enhanced H-atom mobility on Pt are responsible of the better catalytic behaviour of the bimetallic PtNi formulation in the steam reforming of acetone.

1. Introduction

There is an increasing interest in the development of technologies for the conversion of biomass derived hydrocarbons in hydrogen rich gas mixtures as a way to overcome the current technical limitations in hydrogen supply and storage. Recent developments in flash pyrolysis technologies make it possible to convert lignocellulosic biomass efficiently to a bio-oil (a mixture of aliphatic and aromatic oxygenates: aldehydes, ketones, acids, esters, alcohols, sugars, furans, etc.) which is easier for handling and transport [1]. Steam reforming of aqueous bio-oil fractions is therefore an interesting alternative to produce hydrogen in a renewable way. The direct steam reforming of bio-oil generates high amount of undesirable by-products and high coke/oligomer deposition on catalyst, which quickly deactivates it. Therefore, the successful extraction of hydrogen from bio-oils mainly depends on the development of new catalysts with high thermal stability and improved resistance towards coke formation.

Given the influence of the nature of both the metal and support on the catalytic characteristics of supported metals and to fulfil the above requirements, a careful choice of these elements is essential to develop supported catalysts. Due to complexity of steam reforming of bio-oils, reforming of model oxygenate components has been studied in last decades, focusing on acetic acid, acetone or ethylene glycol as the most representative compounds [2–6] in order to establish more clearly the structure-activity correlations on reforming catalysts. Most of the studies reported in literature have been focused on the reforming of acetic acid, whereas acetone steam reforming (Eq. (1)) has been less studied in spite that this compound could be the model of the carbonyl-containing compounds present in bio-oils (ketones and aldehydes).

$$CH_3COCH_3 + 5H_2O \rightarrow 3CO_2 + 8H_2 \quad (1)$$

According to the literature, different catalysts have been used in steam reforming of oxygenated compounds: Ni/CaO–Al_2O_3 [2], Ni/Al_2O_3 [7] Ni–Zn–Al [8], Ni/ZrO_2 [9], Co–Ce/Al_2O_3 and Co–La/Al_2O_3 [10], Pt/CeO_2 and Pt/ZrO_2 [11–14]. Platinum-based catalysts have been the most used systems, however their high cost limit their practical application. Apart of Pt based catalysts, the high C—C bond-breaking activity and the relatively low cost of Ni make

* Corresponding authors.
E-mail addresses: r.navarro@icp.csic.es (R.M. Navarro), jlgfierro@icp.csic.es (J.L.G. Fierro).

0926-860X/$ – see front matter © 2013 Elsevier B.V. All rights reserved.
http://dx.doi.org/10.1016/j.apcata.2013.09.056

it a suitable active phase for oxygenates reforming reactions. However coke formation is an important problem in bio-oil reforming on Ni based catalysts. The platinum group metals have been reported to be more effective catalysts by preventing coke deposition since Pt crystallites do not dissolve carbon. Several authors have reported that the addition of small amounts of noble or semi-noble metals to Ni catalysts improve their catalytic performance decreasing the coke formation on the Ni surfaces [15–18]. The high hydrogenation activity of Pt or Cu could also help the formation of molecular H_2 from atomic H, improving the activity of nickel catalyst in the reforming of bio-oil.

The nature of support also influences the catalytic performance of supported metal catalyst for the steam reforming of oxygenated compounds since it affects both the dispersion and stability of the metal as well as it may participate in the reaction. Among oxide supports, alumina-based supports are often used as a substrate for the reforming catalysts because of their mechanical and chemical resistance under reaction conditions. However, the acid sites of alumina could participate in undesirable reactions during the acetone reforming such as aldol condensation [19] and oligomerization [12] that could form deposits on the catalyst surface. Thus, additives or promoters are often used in reforming catalyst formulations. For this purpose, rare earth elements are extensively used as promoters in the catalysts used in the reforming of oxygenated compounds. In particular, it is described the beneficial effect of lanthanum oxide in the stability of catalysts for steam reforming due to its known capability to remove carbon formation from metallic surfaces [20–22]. Additionally, lanthanum has been reported to prevent the thermal sintering of bare alumina [23].

With this background, in this contribution we study the effect of Pt and Cu addition on the behaviour of Ni catalysts supported on Al_2O_3 modified with lanthanum for acetone reforming (as model molecule of bio-oil). Careful investigation of the structure of catalysts were done in an attempt to establish a relationship between activity and the changes in structural and surface characteristics induced by Pt or Cu addition to Ni catalysts.

2. Experimental

2.1. Catalyst preparation

Lanthanum modified-Al_2O_3 support (15 wt% La_2O_3) was prepared by impregnation of a commercial γ-Al_2O_3 (Alfa Aesar, S_{BET} 235 m^2/g) with 0.09 M aqueous solution of $La(NO_3)_3{\cdot}xH_2O$ (Aldrich 99.9%) using 10 $mL/g_{support}$ as impregnation ratio. Previous to lanthanum impregnation, the Al_2O_3 support was previously stabilized by treating in static air in an oven at 1073 K for 12 h (A). The La-impregnated support (A-La) was dried under static air at 393 K for 3 h and subsequently calcined at 1073 K for 8 h.

Monometallic Ni reference catalyst (Ni/A-La, 12 wt% NiO) was prepared by impregnation of the lanthanum modified-Al_2O_3 support, with 0.16 M aqueous solutions of $Ni(NO_3)_2$ using 10 $mL/g_{support}$ as impregnation ratio. The sample was impregnated for 5 h, subsequently dried at 393 K for 2 h, and finally calcined in air at 773 K for 4 h.

MNi bimetallic catalysts (MNi/A-La, M = Pt or Cu, 1 wt%) were prepared by wet impregnation of the calcined Ni/A-La catalyst with aqueous solutions of the corresponding metal precursors (0.005 M of $Pt(NH_3)_4(NO_3)_2$ or 0.015 $MCu(NO_3)_2$), using 10 $mL/g_{Nicatalyst}$ as impregnation ratio during 2 h. After drying at 383 K for 14 h, the impregnated bimetallic samples were calcined under air at 773 K for 4 h.

2.2. Catalyst characterization

The chemical composition of the catalysts was determined by inductively coupled plasma atomic emission spectroscopy (ICP-AES), using a Perkin-Elmer Optima 3300DV apparatus. The samples were first dissolved in acid solutions (a mixture of HF, HCl and HNO_3), microwaved for 15 min, and diluted to concentrations within the detection range of the instrument.

N_2 adsorption–desorption isotherms were obtained at 77 K over the whole range of relative pressures, using a Micromeritics ASAP 2100 automatic device on samples previously degassed at 423 K for 12 h. BET specific areas were calculated from these isotherms using the BET method and taking a value of 0.162 nm^2 for the cross-section of the physically adsorbed N_2 molecule. The pore size distribution was calculated by applying the Barrer–Joyner–Halenda method (BJH) to the adsorption branch of the N_2 isotherm. The total pore volume was calculated from the adsorption isotherms at $P/P_0 = 0.98$.

Temperature-programmed reduction experiments were carried out on a semiautomatic Micromeritics TPD/TPR 2900 apparatus equipped with a TC detector. Prior to reduction experiments, the samples (about 30 mg) were treated thermally under an air stream at 573 K to remove water and other adsorbed contaminants. TPR profiles were obtained by heating the samples under a 10% H_2/Ar flow (50 mL/min) from 233 to 1173 K at a linearly programmed rate of 10 K/min. The effluent gas was passed through a cold trap to remove water before measuring the amount of hydrogen consumed during reduction by the TC detector. The TCD signals were normalized by the measured weight of each sample.

X-ray powder diffraction patterns were recorded following the step-scanning procedure (step size 0.02°, 2θ scanning from 5° to 90°) using a computerized Seifert XRD 3000P diffractometer (Cu Kα radiation, λ = 0.15418 nm). A rate of 500 s per step was used during a continuous scan in the above mentioned range. Volume-averaged crystallite sizes were determined by applying the Debye–Scherrer equation from the line broadening (β_r) of the characteristic (2 0 0) NiO peak at $2\theta = 43.3°$ and the (2 0 0) Ni-metal peak at $2\theta = 53.8°$ after subtracting the instrument effect ($\beta_r = \sqrt{\beta_0^2 - \beta_i^2}$); β_0 = total line broadening, β_i = instrumental broadening = 0.058 rad).

X-ray photoelectron spectroscopy (XPS) was used to study the chemical composition and oxidation state of the catalyst surfaces. Photoelectron spectra were recorded with a VG Escalab 200R electron spectrometer equipped with a Mg Kα X-ray source ($h\nu = 1253.6$ eV) and a hemispherical electron analyser operating at constant transmission energy (50 eV). The areas of the peaks were estimated by calculating the integral of each peak after subtracting a Shirley background and fitting the experimental peak to a combination of Lorentzian/Gaussian lines of variable proportions. The reduction treatment was carried out ex situ at 823 K in H_2/N_2 (1/9 vol) flow for 90 min followed by re-reduction in situ at 773 K for 30 min. The C 1s, Al 2p, Pt 4d, Ce 3d and Ni 2p core-level spectra were recorded. Differential charging was observed in all samples. This charging effect was corrected by referencing the binding energies (accuracy ± 0.1 eV) to the C 1s signal arising from carbon contamination at 284.8 eV.

Temperature programmed oxidation analyses of spent catalysts were carried out using a thermo-gravimetric analyser (Mettler Toledo TGA/SDTA 851e) to determine the amount of coke deposited on catalysts. The standard protocol involved the weight change of the sample (20 mg) during its heating in 200 mL/min of N_2 as purge gas and 50 mL/min of O_2 as reactive gas from 298 to 1123 K at a heating rate of 10 K/min.

Table 1
Chemical composition (TXRF) and textural properties (N_2 adsorption–desorption isotherms at 77 K) of calcined supports and catalysts.

	Ni (at%)	M (Pt or Cu) (at%)	La (at%)	S_{BET} (m^2/g Al_2O_3)	V_{pore} (cm^3/g Al_2O_3)	D_{pore} (nm)
A	–	–	–	160	0.845	20
A-La	–	–	5.9	147	0.757	21
Ni/A-La	9.2	–	4.2	157	0.694	18
CuNi/A-La	9.2	1.0	4.5	166	0.554	14
PtNi/A-La	9.0	0.2	4.4	166	0.476	12

2.3. Catalytic activity measurements

The samples in reduced form were tested in the steam reforming of acetone (Eq. (1)) under a GHSV = 10,180 h^{-1} at atmospheric pressure with H_2O/CH_3COCH_3 = 6.0 and N_2 = 41 vol%. Activity tests were performed using 0.5 cm^3 of catalyst diluted with SiC (both in the 0.4–0.5 mm particle size range) at a volume ratio of 3:1 to avoid adverse thermal effects. The catalyst bed was supported over a frit quartz plate fixed to the reactor walls. Reaction conditions for catalysts testing were selected in order to achieve high acetone conversion level to know the evolution of the catalyst towards carbon deposits, that is the main phenomenon responsible for catalysts deactivation in this reaction, in a short period of time (24 h). The catalyst bed was placed in a 6 mm ID quartz tubular reactor with a coaxially centred thermocouple. Prior to reaction, the catalysts were flushed in nitrogen at 473 K, followed by reduction in situ at 873 K for 2 h (heating rate 5 K/min) with 50 mL(STP)/min of a 10 vol% H_2/N_2 mixture. The pre-treating gases were flushed from the reactor with N_2 before admission of the acetone/water/N_2 reaction mixture. Acetone–water mixture was fed into the pre-heater by means of syringe pump (Becton-Dickinson) before mixing with a N_2 stream controlled with Brooks model 5850E mass flow controller. Activity was measured at 873 K maintaining the reaction for 12 h in order to check if there was any deactivation of the catalysts. The reaction gas products were analysed on-line by GC with TCD (Agilent) equipped with Porapack Q (CO_2, C_2H_6, C_2H_4, CH_2CO, water and acetone) and molecular sieve 5A (H_2, O_2, N_2, CO) packed columns connected in series, using He as carrier gas. Liquid products were analysed by GC with FID (Varian) and porapack Q capillary column using He as carrier gas.

Activity data were reported as acetone conversion ($X_{C_3H_6O}$), acetone gasification and selectivity to the different gasification products (S_i), which are defined as follows:

$$X_{C_3H_6O}(\%): \quad \frac{(\text{mole } C_3H_6O)_{in} - (\text{mole } C_3H_6O)_{out}}{(\text{mole } C_3H_6O)_{in}} \times 100 \tag{2}$$

$$\text{Gasification}(\%): \quad \frac{\left(\sum \text{mol i}\right)_{out}}{(3\,\text{mole } C_3H_6O)_{in}} \times 100, \quad i = CO,\ CO_2,\ CH_4 \tag{3}$$

$$Si(\%) = \frac{(\text{mole i})_{out}}{\left(\sum \text{mol i}\right)_{out}} \times 100, \quad i = H_2,\ CO,\ CO_2,\ CH_4,\ C_2H_4,\ C_2H_6\ CH_2CO \tag{4}$$

3. Results

3.1. Characterization of fresh catalysts

3.1.1. Chemical composition and textural properties

Table 1 summarizes the chemical composition, expressed as atomic percentages, and the textural properties measured by N_2 adsorption–desorption isotherms for the as-prepared catalysts and supports. For both A-La support and MNi/A-La catalyst, the atomic percentages of La determined by ICP-AES are well correlated with the theoretical values derived from nominal composition (5.2 at% in A-La support and 4.7 at% in MNi/A-La catalysts). Atomic percentages of Ni, Pt and Cu are also close to that expected from nominal composition (Ni = 9.3 at%, Cu = 0.92 at% and Pt = 0.2 at%). The close composition of the catalysts to nominal values indicates the effectiveness of the impregnation method used in the preparation of catalysts.

For the sake of a valid comparison, the N_2 adsorption–desorption data were normalized to unit weight of Al_2O_3 support. As observed in Table 1, the incorporation of a 15 wt% of lanthanum oxide causes a slight decrease in both surface area and pore volume indicative of a partial blockage of the original pores of the Al_2O_3 by lanthanum species. However, the low decrease in surface area observed confirms the capacity of the alumina support to disperse the high lanthanum loading used in the study [23]. The incorporation of Ni to A-La support provokes a slight decrease in pore volume with simultaneous increase in surface area respect to that observed on bare A-La support. This fact indicates a partial blocking of the alumina pores by nickel entities. The increase in the specific area and the simultaneous pore blocking following the addition of nickel suggests that the nickel phase deposited on the alumina support develops some porosity and contributes to the measured specific area. The Cu or Pt incorporation involves a decrease of the pore volume maintaining similar BET surface areas than monometallic Ni/A-La. This fact is indicative of a partial blockage of the mesoporous structure of Ni/A-La with small Cu or Pt particles not affecting to the surface area exposition.

3.1.2. Temperature programmed reduction

The results of the TPR experiments performed on the monometallic and bimetallic catalysts are shown in Fig. 1. The momometallic Ni/A-La reference catalyst showed a broad reduction peak in the 650–1150 K range, which could be decomposed into four components at reduction temperatures of 673, 776, 863 and 1027 K. According to literature studies [24–26], the reduction peak at 673 K is attributed to reduction of NiO species with weak interaction with alumina support, while the reduction peaks appearing at higher temperatures are related to the reduction of highly dispersed non-stoichiometric amorphous nickel aluminate spinels and to a diluted $NiAl_2O_4$-like phase respectively (bulk spinel typically reduces at 1093 K). Apart from these Ni^{2+} species, the Ni/A-La catalyst showed additional hydrogen consumption peaks at 540 K, which could be ascribed to the reduction of small NiO species with weak interaction with the A-La support.

For bimetallic CuNi/A-La catalyst, a complex TPR profile is observed in the temperature range of 373–1173 K. The reduction peaks are associated to the reduction of nickel and copper oxides of different dispersions and interactions with the A-La support. The reduction peak at 479 K is attributed to the reduction of Cu^{2+} species. According to the literature, the reduction of CuO depends on the particle size and dispersion, being lower reduction temperatures to higher dispersion [27,28]. Therefore the reduction peak at 479 K is indicative of the CuO particles highly dispersed on A-La

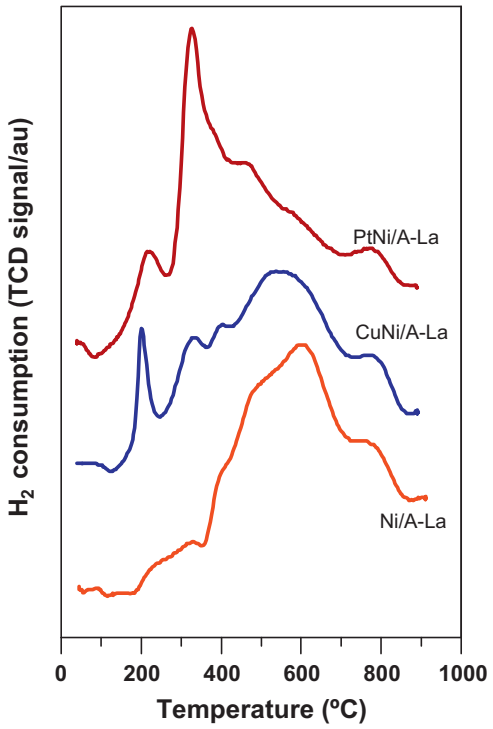

Fig. 1. Temperature-programmed reduction profiles of bimetallic MNi/A-La (M = Cu or Pt) and Ni/A-La (reference) (10 vol% H_2/Ar, heating rate 10 K/min).

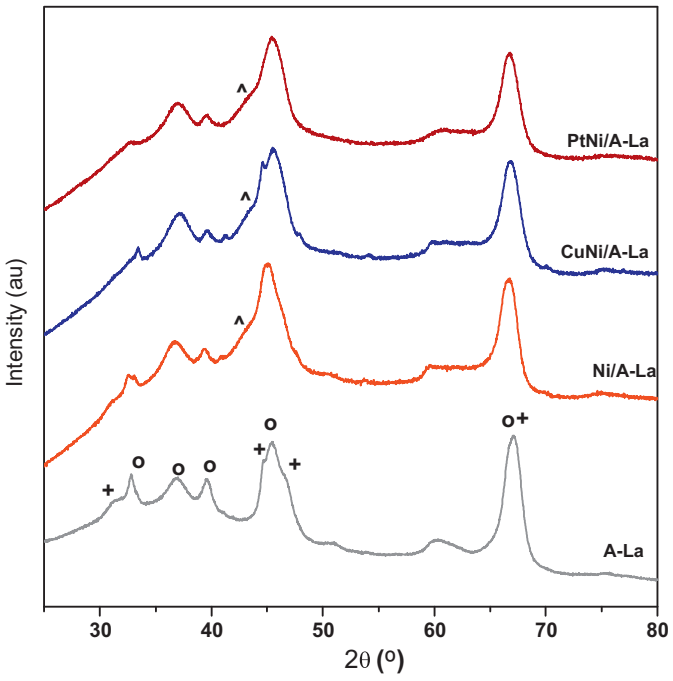

Fig. 2. XRD patterns of bimetallic MNi/A-La (M = Cu or Pt) and Ni/A-La (reference) in calcined state. (o, γ-Al_2O_3; +, θ-Al_2O_3; ; NiO).

support. The second group of peaks observed at higher temperatures is assigned to the reduction of Ni^{2+} species with different degrees of interaction with the Al_2O_3, as well as surface $NiAl_xO_y$. The relative amount of the Ni^{2+} species that can be already reduced at ca. 673 K increases in the proportion with the loading of Cu. However, the reduction temperature of these species does not change significantly respect to that observed on reference Ni/A-La, indicating that the presence of Cu on the surface did not affect significantly the reducibility of Ni^{2+} species.

The reduction profile of bimetallic PtNi/A-La catalyst shows changes respect to the Ni/A-La reference. For the PtNi/A-La catalyst, the most intense H_2 consumption peak is centred at 600 K with a shoulder additional peak at 500 K and a broad peak in the region 743–1100 K. The reduction peak at low temperature comprises the reduction of PtO_x over Al_2O_3 [29]. The consumption peaks observed in the region 600–923 K include the reduction of Ni species with different degrees of interaction with the Al_2O_3, as well as surface $NiAl_xO_y$. It is remarkable that the reduction of this type of Ni^{2+} species was recorded at temperatures ca. 120 K lower than in the Ni/A-La reference catalyst. This phenomenon is attributed to a promoting effect of Pt on the reducibility of Ni species, in good agreement with the literature [30]. Finally, the hydrogen consumption centred at ca. 1050 K appeared unchanged in all the catalysts, indicating that the presence of Pt on the surface did not affect the reducibility of bulk $NiAl_2O_4$.

From the TPR of the catalysts, the activation temperature of catalysts was set at 873 K in order to reduce an important proportion of the Ni^{2+} species with weak and medium interaction with the support and to prevent sintering of Ni metal particles.

3.1.3. X-ray diffraction (XRD)

Fig. 2 shows the XRD patterns of support and as-prepared catalysts. The characteristic peaks of poorly crystalline γ-Al_2O_3 (at 37.4, 46.0 and 68.8 JCPD 29-063) and traces of θ-Al_2O_3 phase (at 31.2°, 36.6° and 67.4° JCPDS 86-1410) were detected in the XRD pattern of the A-La support. No diffraction peaks corresponding to crystalline species of either La_2O_3 (JCPDS 83-1355) or $LaAlO_3$ (JCPDS 85-1071) were observed in the A-La support. This is not surprising because lanthanum exists in the form of a two-dimensional overlayer on alumina, which cannot by detected by XRD for lanthanum loadings up to 8.5 μmol La/m^2 [23].

XRD pattern of the calcined bimetallic catalysts and the Ni/A-La reference showed reflections at 43.3 characteristic of the most intense reflection (2 0 0) of crystalline phase of NiO (JCPDS 78-643). The presence of $NiAl_2O_4$ would be difficult to determine by this technique, since the diffraction lines of this spinel phase are coincident with those of the γ-Al_2O_3 (with pseudospinel structure). No diffraction peaks related to Pt or Cu phases were detected in the bimetallic Pt and CuNi/A-La calcined catalysts. This is due to the low concentration of Pt and Cu in the samples (Table 1) but it could also be a sign of the high dispersion of Pt or Cu species, since no periodic structures higher than 4 nm could be observed by XRD.

The crystalline structure of the reduced catalysts has been also analysed by XRD and the diffraction patterns are displayed in Fig. 3. The XRD profiles of reduced catalysts present reflections corresponding to γ- and θ-Al_2O_3 phases detected in calcined samples. In addition to these phases, the diffraction patterns of the reduced catalysts showed lines at 2θ angles of 44.4 and 53.8 attributed to metallic Ni phase (JCPDS 04-850). On all reduced catalysts, the NiO phase has completely disappeared which indicates the total reduction of the NiO crystallites detected in the calcined catalysts. The XRD patterns of the reduced bimetallic catalysts did not show diffraction peaks related to crystalline reduced phases neither platinum nor copper. As indicated previously, this fact could be associated to the low concentration of Pt and Cu in the samples or be a sign of the high dispersion of Pt or Cu species.

The crystallite size of the phases detected by XRD has been calculated for the catalysts before and after reduction (Table 2). The crystallite size values were estimated by application of Scherrer equation to the most intense diffraction peak of each phase involved (43.3 for NiO and 53.8 for Ni^0). The low XRD reflections corresponding to metallic Ni phases may lead to some inaccuracies in the determination of absolute crystalline sizes. Nevertheless,

Table 2
Average crystallite size of the crystalline phases detected on calcined, fresh reduced and used catalysts from XRD.

	Calcined		Reduced		Used	
	NiO (nm)	MO_x (M = Pt,Cu) (nm)	Ni^0 (nm)	M^0 (M = Cu, Pt) (nm)	Ni^0 (nm)	M^0 (M = Cu, Pt) (nm)
Ni/A-La	8.8	–	9.3	–	15	–
CuNi/A-La	9.9	n.d.	10	n.d.	18	6
PtNi/A-La	9.3	n.d.	9.3	n.d.	11	n.d.

quantitative estimation of crystallite sizes by applying the Scherrer equation after a careful mathematical treatment of diffraction patterns allows achieving the accuracy degree necessary for comparative purposes. A careful deconvolution of the range 2θ 40–50° was done in order to subtract the contribution of diffraction peaks of alumina support to the NiO peak. It can be observed (Table 2) that crystallite size of NiO formed on A-La support was close to 9 nm. The presence of Pt or Cu in bimetallic catalysts did not change the NiO crystallite size observed on monometallic Ni/A-La reference. After reduction, the metallic Ni crystallite sizes are similar to the original NiO crystallites for all the catalysts, not showing therefore sintering of Ni particles during the reduction treatment.

3.1.4. X-ray photoelectron spectroscopy (XPS)

The nature of surface species and composition of the catalysts were evaluated by photoelectron spectroscopy (XPS). The binding energies of Al 2p, La 3d, Cu 2p, Pt 4d, and C 1s core-levels have been recorded for the calcined catalysts and the results are summarized in Table 3. For all catalysts, the La $3d_{5/2}$ peak envelopes were centred at 835.6–835.8 eV. The observed binding energies of La $3d_{5/2}$ are close to the values reported in those studies for well-dispersed lanthanum species on alumina. The XPS spectra of Ni 2p level showed for all the catalysts the characteristic profile of Ni^{2+} species (Fig. 4). As can be seen in Fig. 4, there is partial overlapping between the La 3d and Ni 2p energy regions. Notwithstanding peak deconvolution allowed measure the area of the Ni 2p (and satellite) lines and therefore quantitative measurements were also performed. It can be noted that the two Ni 2p peaks show satellite lines placed on the high binding energy side of the principal lines. As these satellites are the fingerprints of Ni^{2+} ions we can state unambiguously that nickel is incorporated as Ni^{2+} species. In all the samples, Ni $2p_{3/2}$ binding energy is shifted to higher values than that of NiO (854.0 eV). This could be the result of the strong interaction between Ni^{2+} species and the support surface. As it has been observed for other Ni catalysts supported on Al_2O_3, some Ni^{2+} ions react on the alumina surface forming a $NiAl_xO_y$ like-spinel structure [31]. The binding energy of Ni $2p_{3/2}$ level for $NiAl_2O_4$ compound is reported in the literature near to 856.9 eV [32], which is a value much closer to our experimental results. Therefore, an important contribution for the Ni 2p surface signal is due to this like-spinel type species. For the CuNi/A-La catalyst, the most intense peak (Cu $2p_{3/2}$) of the Cu 2p line at a binding energy of 934.7 eV and the appearance of satellite lines on each component of the Cu 2p doublet are conclusive that copper is present as CuO oxide. For the PtNi/A-La catalyst, the Pt 4d level was recorded because the most intense peak (Pt 4f) overlaps with the Al 2p level. As shown in Table 3, the Pt $4d_{5/2}$ peak displays a minor component at 315.4 eV associated to a metal phase (Pt^0) [33], and a major one located at 318.0 eV originated from oxidic platinum species, likely PtO_2 [34]. No interaction between Pt and Cu or Pt and Ni phases was detected by XPS since Ni 2p and Pt 4d or Cu 2p binding energies measured were similar to those registered for monometallic counterparts.

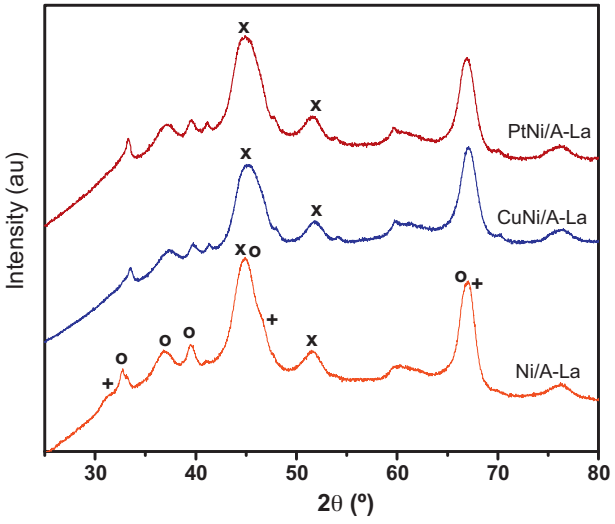

Fig. 3. XRD patterns of bimetallic MNi/A-La (M = Cu or Pt) and Ni/A-La (reference) after reduction. (o, γ-Al_2O_3; +, θ-Al_2O_3, ×, Ni^0).

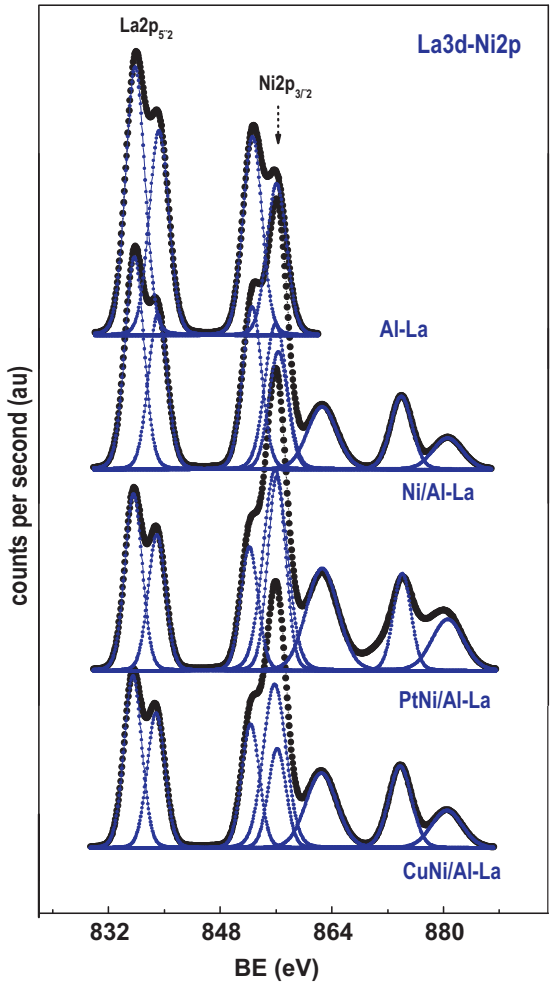

Fig. 4. La3d–Ni2p binding energy region of NiM/A-La and Ni/A-La calcined catalysts.

Table 3
Binding energies (eV) of core-levels and surface atomic percentages derived from XPS measurements of calcined catalysts.

	Al 2p	La $3d_{5/2}$	Ni $2p_{3/2}$	M[a]	Al (at%) (from nom. comp.)	La (at%) (from nom. comp.)	Ni (at%) (from nom. comp.)	M (at%) (from nom. comp.)
A-La	74.5	835.8	–	–	90.4 (93.9)	9.6 (6.1)	–	–
Ni/A-La	74.5	835.8	856.0	–	72.1 (85.0)	15.9 (5.4)	11.9 (9.6)	–
PtNi/A-La	74.5	835.6	856.1	315.4 (38) 318.0 (62)	73.0 (84.5)	7.1 (5.5)	19.6 (9.6)	0.3 (0.3)
CuNi/A-La	74.5	835.5	855.9	934.7	75.0 (84.0)	7.3 (5.5)	13.7 (9.6)	3.9 (0.9)

[a] Pt $4d_{5/2}$ or Cu $2p_{3/2}$.

Table 4
Binding energies (eV) of core-levels and surface atomic ratios from XPS analysis of H_2-reduced catalysts.

	Al 2p	La $3d_{5/2}$	Ni $2p_{3/2}$	M[a]	Al (at%) (from nom. comp.)	La (at%) (from nom. comp.)	Ni/Ni^0 (at%) (from nom. comp.)	M (at%) (from nom. comp.)
Ni/A-La	74.5	835.3	852.8 (41) 856.0 (59)	–	83.5 (85.0)	9.6 (5.4)	6.9/2.8 (9.6)	–
CuNi/A-La	74.5	835.3	852.7 (47) 855.9 (53)	932.0	86.2 (84.0)	6.2 (5.5)	5.5/2.6 (9.6)	2.0 (0.9)
PtNi/A-La	74.5	835.3	852.8 (61) 855.7 (39)	314.8	83.1 (84.5)	9.4 (5.5)	7.4/4.5 (9.6)	0.12 (0.3)

[a] Pt $4d_{5/2}$ or Cu $2p_{3/2}$.

The surface atomic ratios of the calcined samples, calculated from the intensities of the XPS peaks are also summarized in Table 3. The homogeneous dispersion of lanthanum on the alumina surface observed for the A-La support is corroborated by the close atomic percentage of La obtained from XPS with respect to the predicted value derived from their nominal composition. The surface XPS La atomic percentage for the Ni/A-La catalyst was substantially higher than in the A-La support, indicating solubilization of a minor fraction of the La-phase along the impregnation with Ni and further precipitation on the external surface during the drying step. In the Ni/A-La catalyst, the calculated Ni atomic surface concentration was similar to the expected value derived from its chemical composition, indicating the homogeneous dispersion of nickel on the A-La support surface. The value of this XPS Ni surface concentration increases for the bimetallic PtNi/A-La catalyst, indicating some redistribution of Ni species on the external surface of catalyst during the second impregnation with Pt. In this sample, it was observed a homogeneous dispersion of Pt achieving a surface concentration close to the value expected from its Pt nominal concentration. In contrast, the bimetallic CuNi/A-La catalyst showed similar Ni surface concentration than that observed on monometallic reference and a Cu surface concentration higher than the expected value, indicating the presence of an overlayer of copper species.

The chemical state and relative proportion of catalysts constituents after reduction were also determined by photoelectron spectroscopy (Table 4). Ni 2p level in reduced samples showed binding energies characteristic of Ni^0 (852.6 eV) [35] and Ni^{2+} ions in nickel aluminate entities (856.2 eV). It can be observed that the amount of metallic Ni at the surface slightly increases in the bimetallic CuNi catalyst. A significant increment was achieved in the bimetallic Pt–Ni catalyst, in good agreement with TPR results. For reduced PtNi catalyst, the binding energy of Pt $4d_{5/2}$ level was observed at 314.8 eV which is a value characteristic of metallic Pt. The peak fit of the Cu $2p_{3/2}$ core level revealed a binding energy at 932.0, which it is assigned to a $Cu^{(0/+1)}$ state [36]. No shift in the binding energy or Pt 4d or Cu 2p levels was observed, and therefore effects like metal–support interaction, i.e., the electron transfer between the Pt or Cu metals and the support or nickel can be ruled out. The surface atomic ratios on reduced catalysts, calculated from the intensities of the peak normalized by atomic sensitivity factors are also summarized in Table 4.

After reduction, it is observed in all catalysts that the Ni surface concentration decreased respect to the values observed in calcined state. This effect has been typically observed for Ni catalysts supported on Al_2O_3, and it is explained by a 'decoration' of metallic particles by dispersed species from alumina support after reduction of surface $NiAl_xO_y$ layer covering the NiO crystallites [37]. It can be observed that the surface concentration of Ni^0 species at the surface varies in bimetallic samples. A significant increase in Ni surface concentration is observed in bimetallic PtNi catalysts while in the case of bimetallic CuNi sample, the surface concentration of metallic Ni was lower than those calculated for the monometallic Ni/A-La reference. After reduction, the XPS Pt and Cu surface concentrations were slightly lower than those obtained from the fresh calcined samples indicating some transformation in particle size or shape of the Pt and Cu oxides during the reduction process.

4. Catalytic activity

To evaluate the contribution of the thermal decomposition of acetone, the homogeneous (non-catalytic) steam reforming of acetone at 873 K was firstly investigated. Under the steam reforming conditions, acetone was converted in small extent (3.3%). The main products observed from the thermal conversion of acetone were methane and ketene (results not shown here). The presence of both products suggests the small participation of the cracking process (Eq. (2)) at the reaction temperature of 873 K in the presence of steam. Small amount of coke (<0.05%) was observed demonstrating that acetone was thermally decomposed to coke to a limited extent under steam reforming conditions used in this study.

$$CH_3COCH_3 \rightarrow CH_2CO + CH_4 \quad (5)$$

The conversion and gasification percentage of acetone for the steam reforming of acetone over monometallic Ni/A-La and bimetallic MNi/A-La catalysts are summarized in Table 5 and plotted in Fig. 5. All catalysts showed complete conversion of acetone

Table 5
Acetone conversion and gasification percentage (to H_2, CO, CO_2 and CH_4) in acetone steam reforming after 10 h on-stream (873 K, $H_2O/CH_3COCH_3 = 6.0$, GHSV = 10,180 h^{-1}).

	Acetone conv. (%)	Gasification (%)
Ni/A-La	100	94.1
PtNi/A-La	100	99.8
CuNi-/A-La	100	56.5

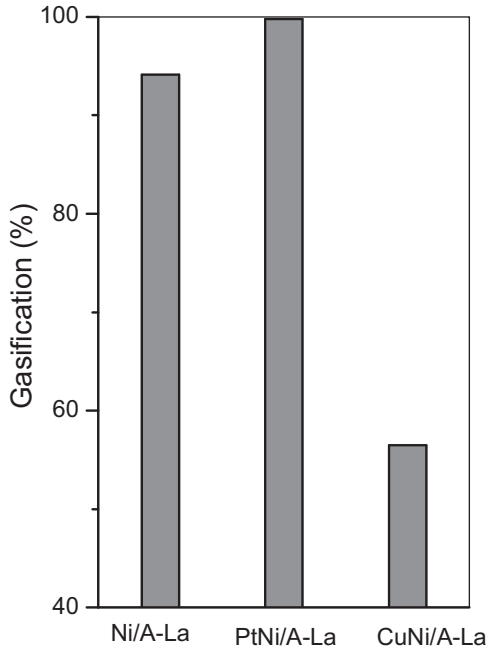

Fig. 5. Gasification of acetone (to H_2, CO_2, CO and CH_4) in the acetone steam reforming (873 K, H_2O/CH_3COCH_3 = 6.0, GHSV = 10,180 h^{-1}).

being H_2, CO, CO_2 and CH_4 the only gas products detected. The higher gasification capacity observed over all catalysts respect to that corresponding to homogeneous thermal reforming remarks the active role of metal sites (Ni, Cu or Pt) in the mechanism of the reforming of acetone. Nevertheless, differences on gasification capacity and gas product distribution were observed on tested catalysts.

It was observed that the monometallic Ni/A-La reference catalyst converted acetone into H_2, CO_2, CO and CH_4 in great extent (94.1%) with some formation of coke/oligomer products (5.9%). On comparing with Ni/A-La reference catalyst, the bimetallic PtNi/A-La sample showed almost complete transformation of acetone (99.8%) into H_2, CO, CO_2 and CH_4 with low coke/oligomer formation (0.2%). On the contrary, the addition of Cu to Ni/A-La catalyst decreases the capacity of the catalysts to transform the acetone into H_2, CO, CO_2 and CH_4, with only the 56.5% of acetone gasified to reforming products. Analysis of liquid products obtained on CuNi catalysts shows the formation of isopropanol, C6, C9 and C12 ketones. The differences in the gasification capacity of the tested catalysts (Fig. 5) imply that incorporation of Pt- and Cu- to Ni modifies in different way the routes of formation of coke/oligomer products observed on monometallic Ni reference catalyst. Formation of coke/oligomer products during the acetone steam reforming arises mainly from catalytic routes since, as indicated previously, coke formation from homogeneous thermal routes is produced at limited extent. Acetone can undergo aldol condensation and oligomerization reactions on catalysts with acidic and/or basic sites as well as hydrogenation metallic sites [38]. Aldol condensation of acetone to diacetone alcohol (DAA) is catalysed by either basic or acid sites, while the dehydration of diacetone alcohol (DAA) to mesityl oxide (MO) is acid-catalysed and the selective hydrogenation of mesityl oxide (MO) requires metal sites [39,40]. At high temperatures, these products can suffer secondary oligomerization reactions leading to numerous higher condensation products which form deposits on the catalysts surface.

Evolution of the selectivity to gas products also depends on catalyst formulation (Fig. 6). Gas produced over Ni/A-La catalyst was a mixture of H_2, CO_2, CO and CH_4 whose composition was

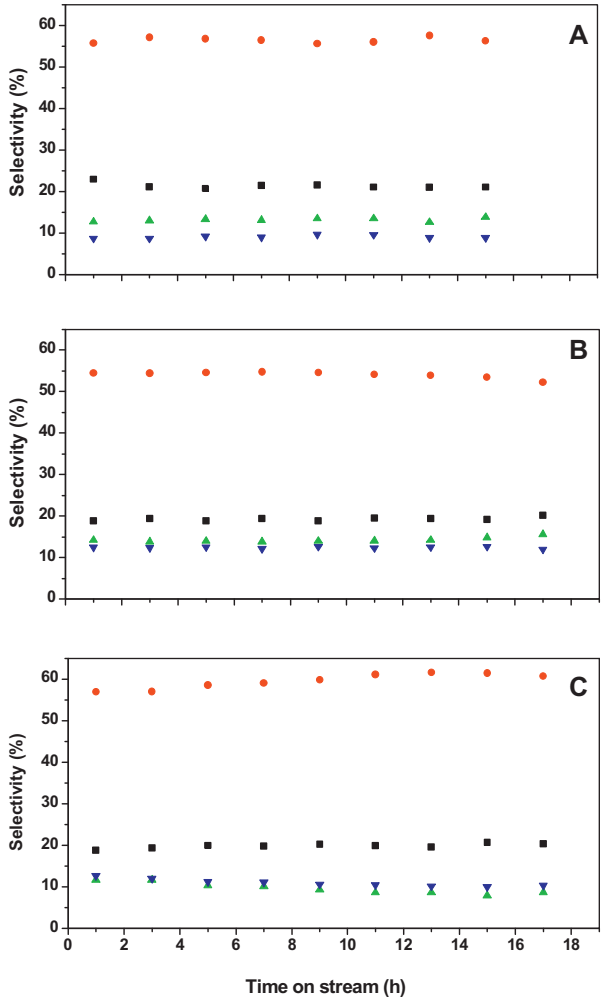

Fig. 6. Selectivity to gas products in acetone steam reforming (873 K, H_2O/CH_3COCH_3 = 6.0, GHSV = 10,180 h^{-1}) over catalysts: (A) Ni/A-La, (B) PtNi/A-La and (C) CuNi/A-La. Selectivity to products (●) H_2, (■) CO_2, (▲) CH_4 and (▼) CO.

approached the values predicted from equilibrium calculations [3]. This indicates that reforming and water gas shift are the main reactions operating over this catalyst. The bimetallic PtNi catalyst showed lower hydrogen selectivity with higher selectivity to CO and CH_4 than that observed for the monometallic Ni/A-La reference catalyst (Fig. 6). This product distribution was indicative of the lower water gas shift capacity of the bimetallic PtNi catalyst respect to the monometallic Ni counterpart. On the other hand, the bimetallic CuNi catalyst showed the highest hydrogen selectivity with lower selectivity to C1 products among the catalyst tested. This fact indicates that in spite of the lower gasification capacity showed by the CuNi/A-La catalyst, the presence of Cu improves the production of hydrogen indicative of an enhancement in the C—H bond breaking and water gas shift capacity respect to the monometallic Ni reference catalyst.

5. Characterization of used catalysts

5.1. X-ray diffraction

The X-ray diffraction profiles of catalysts used for 12 h in the steam reforming of acetone are displayed in Fig. 7. The XRD profiles of used catalysts present reflections corresponding to γ-Al_2O_3, θ-Al_2O_3 and reduced Ni^0 phases which were previously detected in fresh reduced catalysts (Fig. 3). In addition to these phases, the

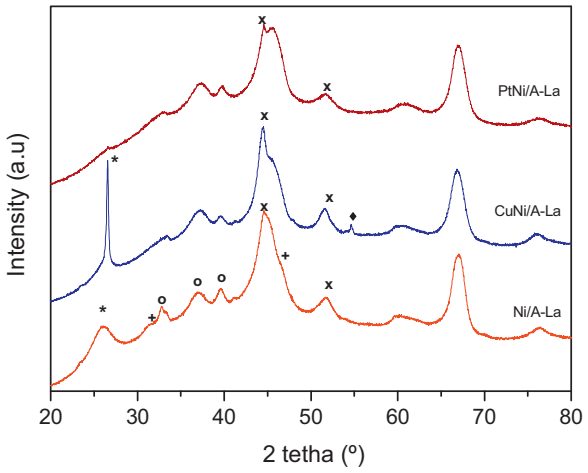

Fig. 7. X-ray diffraction patterns of used catalysts in acetone steam reforming (o, γ-Al_2O_3; +, θ-Al_2O_3; ×, Ni^0; *, graphite; ♦, Cu^0).

diffraction patterns of the used Ni/A-La and CuNi/A-La catalysts showed lines at $2\theta = 26^\circ$ characteristic of graphitic carbon (JCPDS 75-1621). This fact indicates that coke deposition took place during the acetone steam reforming over these catalysts, especially in the case of the bimetallic NiCu catalyst. On the contrary, the bimetallic PtNi catalyst did not show diffraction peaks related to graphitic carbon indicating the limited amount of carbon formed on this sample. Regarding to evolution of Ni^0 species in reaction, it is observed that the corresponding (1 1 1) diffraction lines of metallic nickel at $2\theta = 44.8^\circ$ are more intense after reaction. Based on this observation, some sintering of the Ni^0 crystallites under reaction conditions can be expected. Crystallite sizes of metallic nickel in the used catalysts obtained by applying the Scherrer equation are summarized in Table 2. The size of metallic Ni crystallites observed for monometallic Ni- and bimetallic CuNi-catalysts showed a crystalline size larger than reduced fresh samples, pointing that sintering of metallic Ni crystallites has occurred under reforming conditions on these catalysts. In the case of bimetallic PtNi, the size of Ni crystallites did not significantly change during reaction indicating that the presence of platinum on catalysts prevents sintering of Ni crystallites during the steam reforming reaction.

5.2. Thermogravimetric oxidation

Thermogravimetric analyses of the used catalysts were carried out to calculate the amount of carbonaceous residues retained in the catalysts after reaction by measuring the weight loss during its temperature-programmed oxidation under a 20% O_2 gas flow. In Fig. 8 are represented the TG-TPO profiles (as derivative of the weight loss) of the catalysts used in acetone steam reforming reaction. The derivative TG-TGO profile observed on all used catalysts, with two main contributions, indicates that carbon deposits of different nature were formed on used catalysts. All the used catalysts showed a weight loss in the temperature range 673–973 K. TPO-TG analyses of used catalysts, represented in Fig. 8, show two main oxidation peaks at 773 and 853 K. Oxidation peaks at low temperature can be ascribed to filamentous carbon on metal surfaces [41] whereas the peaks at temperatures higher than 823 K are ascribed to oxidation of more ordered carbon in the form of uniform coke coatings on support [42]. As it is observed in Fig. 8, most of the coke deposited on Ni/A-La catalyst was in the form of graphitic coke (872 K) while for bimetallic CuNi/A-La one it was in the form of filamentous coke on metal surfaces (773 K). For PtNi/A-La catalyst, the formation of carbon is markedly suppressed as indicated by the lower intensity of its oxidation peaks. Coke deposits on used

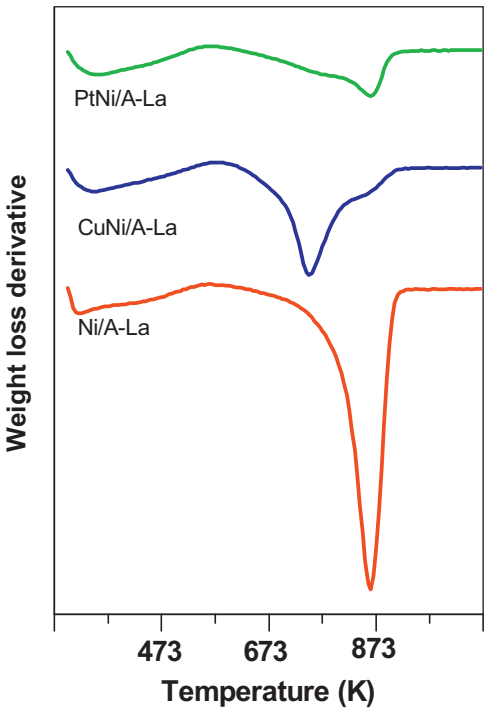

Fig. 8. TG-TPO profiles of used catalysts in acetone steam reforming.

catalysts, summarized in Table 6, show that total amount of coke deposited on catalyst only significantly decreases in the case of the bimetallic PtNi catalyst formulation.

6. Discussion

The acidic/basic properties of the A-La support may participate in the reforming mechanism of acetone since this molecule could react on these sites and reacts towards to diacetone alcohol, mesityl oxide or other products by means of condensation/oligomerization reactions [38–40]. Nevertheless taking into account that all catalysts are supported on the same support, the differences in the characteristics of active metals supported on A-La play an essential role in the catalytic behaviour of the studied samples. The role of metallic sites on reforming reactions of organic molecules is to activate the molecules though O—H, —CH_2—, C—C and CH_2 bond breaking, and to promote the reaction between the organic fragments with the OH groups from the water reagent.

Monometallic Ni/A-La catalyst showed high reforming capacity as it gasifies 94% of the acetone feed (Table 5 and Fig. 5). The high extent of the gasification reactions indicates that reaction routes based on condensation/oligomerization of acetone on support neither proceed to a great extent nor the products formed by these reactions are sequentially fully reformed. Characterization results on Ni/A-La catalyst showed homogeneous dispersion of La_2O_3 on the Al_2O_3 support with good metallic Ni surface exposure, which according to reforming chemistry on Ni catalysts, may be the cause of the high reforming activity of this catalyst as consequence of the enhancement in the C—H and C—C bond activation associated with

Table 6
Carbon deposits on used catalysts after 24 h in acetone steam reforming quantified by TG-TPO analysis.

	mol coke formed/mol C fed (%)
Ni/A-La	1.3
PtNi/A-La	0.6
CuNi/A-La	1.1

low size metal crystallites [43] and the assistance of lanthanum species in preventing coke deposition [44,45].

According to XRD and XPS results, interactions between Pt or Cu and Ni phases are very weak in the reduced bimetallic catalysts. In spite of this fact, when bimetallic catalysts are compared with monometallic Ni counterpart (Figs. 5 and 6), it is observed that the presence of Cu and Pt has an important effect in the gasification capacity and selectivity of the catalysts. TPR profiles (Fig. 1) showed enhanced reducibility of Ni species on bimetallic catalyst containing platinum. This phenomenon has been observed by several authors and could be explained by hydrogen-spillover on metallic surfaces which may provide high mobility of H-atoms along the catalyst surface that favours the reduction of oxidized species of Ni [33]. XPS analyses on fresh reduced catalysts are in line with above commented TPR results. As observed in Table 4, the bimetallic PtNi catalyst showed higher percentage of metallic nickel species compared with the monometallic counterpart. The changes in the reducibility and exposure of metallic Ni in the bimetallic samples imply variations in the surface Ni^0 content of the catalysts after reduction. A significant increase in Ni^0 surface concentration is observed in bimetallic PtNi catalysts while in the case of bimetallic CuNi sample, the surface concentration of metallic Ni was lower than that determined for the monometallic Ni/A-La reference. The gasification capacity of bimetallic catalysts (Table 5 and Fig. 5) clearly indicated a better performance of the bimetallic PtNi catalyst as compared to bimetallic CuNi counterpart. A much lower degree of gasification was observed for the bimetallic CuNi catalyst respect to the monometallic Ni counterpart.

According to the literature, the activity for hydrocarbon reforming reactions on Ni based catalysts is roughly proportional to metallic nickel surface area for a wide number of supports [46]. However, if a comparison is made between the gasification capability of the bimetallic catalyst with the exposure of metallic Ni in reduced catalysts, it can be inferred that properties other than surface exposure of metallic Ni affect the reforming activity of bimetallic catalysts. In this scenario, the intrinsic reforming activity of Pt and Cu might play a role in the catalytic behaviour of the bimetallic catalysts studied here. Studies on reforming over CuNi catalysts have shown that the promotion of activity in is associated with the modification of the Ni ensemble environment by forming NiCu alloy [47–49]. The TPR profile, XRD and XPS analyses of the reduced CuNi/A-La catalyst did not reveal the formation of CuNi alloy. Therefore, the low gasification capacity of the bimetallic CuNi catalyst suggests changes in the acetone reaction mechanism associated to the presence of metallic Cu since this metal is not active for C—C bond breaking as Ni or Pt are. The lower reforming capacity of the CuNi catalysts is hypothesized to be associated with the a loss of selectivity due to the formation of isopropanol by direct hydrogenation of acetone under metallic copper sites because it is known that acetone undergoes this hydrogenation reaction easily in the presence of metallic copper [50,51]. Analysis of liquid products obtained over this catalyst confirms this fact.

The reforming activity of bimetallic PtNi catalyst shows that addition of platinum enhances the gasification capacity respect to monometallic Ni counterpart (Table 5, Figs. 5 and 6) achieving the bimetallic formulation almost complete gasification of acetone. The higher gasification activity observed for PtNi sample suggests that the capacity of this catalyst in the C—C and C—H bond activation is higher than that of monometallic counterpart. According to the TPR and XPS analyses, the presence of Pt modifies the interactions between nickel species and A-La support, leading to differences in the reducibility and surface concentration of reduced nickel species. As discussed above, higher nickel surface concentration implies higher number of sites for C—C and C—H bond activation during hydrocarbon steam reforming and therefore this fact is, in part, responsible of the better reforming behaviour observed for the bimetallic PtNi catalyst. The improvement in reforming activity can be also originated by the differences in coke formation and resistance to thermal sintering observed when Pt is present in the catalyst formulation. As observed from XRD profiles of used catalysts (Fig. 7 and Table 2), the degree of sintering of nickel crystallites after reaction is substantially lower in the case of the bimetallic PtNi catalyst respect to monometallic Ni one. As it is seen in Table 6, a lower amount of carbonaceous deposit was observed in bimetallic PtNi formulation. This observation indicates that Pt species are involved in the gasification of coke precursors. It is know that both the metallic Ni particle size ant the Pt play a major role in assisting coke removal. In this sense, Ni particles of larger size favour carbon deposition while platinum assists in coke removal by means of a cooperative effect of both Pt and Ni phases [52]: Ni provides activity in C—C and C—H bond activation and Pt particles enhance the mobility of the H-atoms formed in the reaction, helping the gasification of coke intermediates (C_xH_y) formed during the reforming.

7. Conclusions

The steam reforming of acetone (as model molecule of bio-oil) over bimetallic PtNi and CuNi catalysts supported on La-modified Al_2O_3 has been investigated with respect to the structural and morphological characteristics of the dispersed metallic phases. The activity of bimetallic catalysts clearly indicated the better performance of bimetallic PtNi catalyst in terms of gasification capacity and resistance to coke deposits as compared to the bimetallic CuNi counterpart. A much lower degree of gasification as well as lower selectivity to CO and CO_2 was observed for Cu-based bimetallic catalyst respect to monometallic Ni one. Characterization analyses of the reduced CuNi/A-La catalysts revealed a poor interaction Cu-Ni with no formation of CuNi alloy. Therefore, the low gasification capacity of the bimetallic CuNi catalyst suggests changes in the acetone reaction mechanism due to the formation of isopropanol by direct hydrogenation of acetone under metallic copper. The reforming activity of bimetallic PtNi catalyst shows that addition of platinum to nickel enhances the gasification capacity respect to the monometallic Ni counterpart, achieving the bimetallic catalyst almost complete gasification of the acetone. The characterization results over bimetallic PtNi catalyst revealed that the presence of platinum increases the reducibility and surface exposure of metallic Ni. Additionally, the better ability of Pt to enhance the mobility of the H-atoms formed in the reaction could help the gasification of carbon precursors. The combination of both effects is interpreted as responsible for the higher reforming capacity of the bimetallic PtNi catalyst.

Acknowledgements

This research was supported by the Ministry of Science and Innovation (Spain) and the Autonomous Government of Madrid, Madrid (Spain) under grants ENE2010-21198-C04-01 and S2009ENE-1743, respectively. Partial support to this work came from Najran University, The Kingdom of Saudi Arabia.

References

[1] X. Hu, L. Zhang, G. Lu, Appl. Catal. A: Gen. 427 (2012) 49.
[2] E.Ch. Vagia, A.A. Lemonidou, Appl. Catal. A: Gen. 351 (2008) 111–121.
[3] E.Ch. Vagia, A.A. Lemonidou, Int. J. Hydrogen Energy 32 (2) (2006) 212–223.
[4] K. Takanabe, K. Aika, K. Seshan, L. Lefferts, Chem. Eng. J. 120 (2006) 1133–1137.
[5] C. Rioche, S. Kulkarni, F.C. Meunier, J.P. Breen, R. Burch, Appl. Catal. B: Environ. 61 (2005) 130–139.
[6] C. Resini, L. Arrighi, M.C.H. Delgado, M.A.L. Vargas, L.J. Alemany, P. Riany, R.M. Berardinelli, G. Busca, Int. J. Hydrogen Energy 31 (1) (2006) 13–19.
[7] P.N. Kechagiopoulos, S.S. Voutetakis, A.A. Lemonidou, I.A. Vasalos, Energy Fuels 20 (2006) 2155–2163.

[8] L. Barattini, G. Ramis, C. Resini, G. Busca, M. Sisani, U. Costantino, Chem. Eng. J. 153 (2009) 43–49.
[9] Z. Li, X. Hu, L. Zhang, S. Liu, G. Lu, Appl. Catal. A: Gen. 417–418 (2012) 281–289.
[10] X. Hu, G. Lu, Catal. Commun. 12 (2010) 50–53.
[11] B. Matas Güell, I. Babich, K.P. Nichols, J.G.E. Gardeniers, L. Lefferts, K. Seshan, Appl. Catal. B: Environ. 90 (2009) 38–44.
[12] K. Takanabe, K. Aika, K. Seshan, L. Lefferts, J. Catal. 227 (2004) 101–108.
[13] K. Takanabe, K. Aika, K. Inazu, T. Baba, K. Seshan, L. Lefferts, J. Catal. 243 (2006) 263–269.
[14] K. Takanabe, K. Aika, K. Seshan, L. Lefferts, Top. Catal. 49 (2008) 68–72.
[15] J.A. Rodriguez, Surf. Sci. Rep. 24 (1996) 225–287.
[16] J.C. Zhang, Y.H. Wang, R.Y. Ma, D.Y. Wu, Appl. Catal. A: Gen 243 (2003) 251–259.
[17] M. Arai, T. Ebina, M. Shirai, Appl. Surf. Sci. 148 (1999) 155–163.
[18] V.R. Choudhary, B. Prabhakar, A.M. Rajput, J. Catal. 157 (1995) 752–754.
[19] W.T. Reichle, J. Catal. 63 (1980) 295–306.
[20] A. Iriondo, V.L. Barrio, J.F. Cambra, P.L. Arias, M.B. Güemez, R.M. Navarro, M.C. Sanchez-Sanchez, J.L.G. Fierro, Catal. Commun. 10 (8) (2009) 1275–1278.
[21] A. Iriondo, V.L. Barrio, J.F. Cambra, P.L. Arias, M.B. Guemez, R.M. Navarro, M.C. Sanchez-Sanchez, J.L.G. Fierro, Top. Catal. 49 (1–2) (2008) 46–58.
[22] M.C. Sanchez-Sanchez, R.M. Navarro, J.L.G. Fierro, Catal. Today 129 (3–4) (2007) 336–345.
[23] M. Bettman, R.E. Chase, K. Otto, W.H. Weber, J. Catal. 117 (1989) 447–454.
[24] J.M. Rynkowski, T. Paryjczak, M. Lenik, Appl. Catal. A: Gen. 106 (1993) 73–80.
[25] N. Ichikuni, D. Murata, S. Shimazu, T. Uematsu, Catal. Lett. 69 (2000) 33–37.
[26] J.T. Richardson, M.W. Twigg, Appl. Catal. A: Gen. 167 (1998) 57–69.
[27] C.H. Tu, A.Q. Wang, M.Y. Zheng, X.D. Wang, T. Zhang, Appl. Catal. A: Gen. 297 (2006) 40–51.
[28] X.C. Zheng, S.H. Wu, S.P. Wang, S.R. Wang, S.M. Zhang, P. Huang, Appl. Catal. A: Gen. 283 (2005) 217–226.
[29] C. Hwang, C. Yeh, J. Mol. Catal. A: Chem. 112 (1996) 295–303.
[30] J.M. Rynkowski, T. Paryjczak, M. Lenik, M. Farbotko, J. Goralski, J. Chem. Soc. Faraday Trans. 91 (1995) 3481–3492.
[31] P. Salagre, J.L.G. Fierro, F. Medina, J.E. Sueiras, J. Mol. Catal. A: Chem. 106 (1996) 125–132.
[32] NIST X-ray Photoelectron Spectroscopy Database: Version 3.4. National Institute of Standards and Technology, Gaithersburg, 2002, Available in: http://srdata.nist.gov/xp
[33] A.S. Ivanova, S.M. Slavinskaya, R.V. Gulyaev, V.I. Zaikovskii, O.A. Stonkus, I.G. Danilova, L.M. Plyasova, I.A. Polukhina, A.I. Boronin, Appl. Catal. B: Environ. 97 (1–2) (2010) 57–66.
[34] T. Huizinga, J. Vangrondelle, R. Prins, Appl. Catal. 10 (1984) 199–211.
[35] F. Devred, A.H. Gieske, N. Adkins, U. Dahlborg, C.M. Bao, M. Calvo-Dahlborg, J.W. Bakker, B.E. Nieuwenhuys, Appl. Catal. A: Gen. 356 (2009) 154–162.
[36] C.C. Chusuei, M.A. Brookshier, D.W. Goodman, Langmuir 15 (1999) 2806–2808.
[37] Y.J. Huang, J.A. Schwarz, J.R. Diehl, J.P. Baltrus, Appl. Catal. 37 (1988) 229–234.
[38] A.A. Nikolopoulos, B.W.-L. Jang, J.J. Spivey, Appl. Catal. A: Gen. 296 (1) (2005) 128–136.
[39] Y. Higashio, T. Nakayama, Catal. Today 28 (1996) 127–136.
[40] N.N. Das, S.C. Srivastava, Bull. Mater. Sci. 25 (4) (2002) 283–292.
[41] S. Wang, G.Q.M. Lu, Appl. Catal. B: Environ. 16 (3) (1998) 267–277.
[42] S. Natesakhawat, R.B. Watson, X. Wang, U.S. Ozkan, J. Catal. 234 (2) (2005) 496–508.
[43] D.L. Trimm, Cat. Rev.-Sci. Eng. 16 (1977) 155.
[44] Y.H. Hu, E. Ruchenstein, Catal. Lett. 36 (1996) 145–152.
[45] Z.L. Zhang, X.E. Verykios, J.M. MacDonald, S. Affrosman, J. Phys. Chem. 100 (1996) 744–751.
[46] J.R. Rostrup-Nielsen, in: J.R. Anderson, M. Boudart (Eds.), Catalysis, Science and Technology, vol. 5, Springer-Verlag, Berlin, 1984.
[47] Z. Xie, C. Xia, M. Zhang, W. Zhu, H. Wang, J. Power Sources 161 (2006) 1056–1061.
[48] J.-H. Lee, E.-G. Lee, O.-S. Joo, K.-D. Jung, Appl. Catal. A 269 (2004) 1–6.
[49] A. Sin, E. Kopnin, Y. Dubitsky, A. Zaopo, A.S. Aricò, D. La Rosa, L.R. Gullo, V. Antonucci, J. Power Sources 164 (2007) 300–305.
[50] J. Cunningham, J.N. Hickey, Z. Wang, Int. J. Energy Res. 20 (1996) 763–766.
[51] J. Cunningham, J.N. Hickey, M.M.D. Brown, B.J. Meenan, J. Mater. Chem. 7 (1993) 743–750.
[52] M.C. Sanchez-Sanchez, R.M. Navarro, D.I. Kondarides, X.E. Verykios, J.L.G. Fierro, J. Phys. Chem. A 113 (2010) 3873–3879.